Journal of Materials Science: Materials in Electronics (2018) 29:11712–11718
https://doi.org/10.1007/s10854-018-9269-8

Preparation and characterization of (100 – x) TiO_2 + (x)ZnO nanocomposites for dye-sensitized solar cells using *Beta vulgaris* and *Syzygium cumini* natural dye extract

S. Kiran[1] · T. Ramesh[2] · S. R. Murthy[1]

Received: 28 December 2017 / Accepted: 10 May 2018 / Published online: 16 May 2018

Abstract
The present paper attempts to report the preparation of TiO_2–ZnO nanocomposite photoanode materials for dye-sensitized solar cells (DSSC) and analyse the efficiency of DSSC with natural dyes. The structural and optical characteristics of the composites were studied by transmission electron microscopy, X-ray diffraction, field effective scanning electron microscopy, energy dispersive spectrometry, photoluminescence and absorption spectroscopy. The synthesized nanocomposites formed on FTO substrates are applied as photoanode in a dye-sensitized solar cell (DSC). The natural dyes extracted from *Beta vulgaris* (Beetroot) and *Syzygium cumini* (black plum) were used in the fabrication of DSSC. The solar cells' photovoltaic performance in terms of short-circuit current, open circuit voltage, fill factor and energy conversion efficiency was tested with photocurrent density–voltage measurements. The evolution of the solar cells parameters is explored as a function of the photoanode and type of dye used in DSSC fabrication.The obtained results show that the efficiency of DSSC significantly changes with the addition of ZnO to TiO_2, while the *Beta vulgaris* dye has evidently shown higher photo sensitized performance compared to *Syzygium cumini* in the preparation of DSSC.

1 Introduction

In recent years, the development of dye-sensitized solar cells (DSSCs) has attracted much attention of researchers due to their environmental friendliness, ease of fabrication and cost-effectiveness [1–5]. A DSSC is consists of a photo-anode (semiconductor electrode), absorbed dye, a counter electrode and an electrolyte containing iodide and triiodide ions [6, 7]. In DSSCs, the photo-anode plays a crucial role in absorbing sunlight and converting solar energy into electric energy. An ideal photo-anode for DSSCs should have features of high specific surface area, high loading of dye molecules, fast electron transport and less interfacial electron recombination [7]. Intensive work has been devoted to the development of TiO_2 based photo-anodes due to its unique properties like, high bandgap (3.2 eV for anatase), chemically inert, photocorrosion stability, as well as inexpensive. However, the sluggish electron mobility and high electron–hole recombination process limit the efficiency of TiO_2 during photo degradation [8]. Many attempts were made to overcome the limitation in the efficiency of the TiO_2 based DSSC such as the fabrication of bi-layer electrode [9, 10], preparation of composite semiconductor photo-anode, use of different dyes etc. [11–14]. In this process, the coupling of various semiconductors has been proposed for the design of composite photoanode to decrease the rate of recombination regarding individual semiconductors. Therefore, to explore efficient photo-anode materials, efforts have been made to utilize bi-functional materials including ZnO/TiO_2 [15], SnO_2/TiO_2 [16], ZnO/SnO_2 [17], $SrTiO_3$/TiO_2 [18]. Particularly, ZnO based composites has attracted great attention due to its high electron mobility (~ 100 cm^2 V^{-1} s^{-1}), thermal conductivity and bandgap (3.3 eV) [19].

Herein, we report the microwave hydrothermal preparation of TiO_2–ZnO composite as the photoanode in DSSC for the enhancement of the energy-conversion efficiency. After the structural, morphological and optical characterization, DSSCs have been fabricated using TiO_2–ZnO composite semiconductor electrode and sensitized using the extracts of

✉ T. Ramesh
ramanasarabu@gmail.com; rameshouphysics@gmail.com

[1] Department of Physics, Osmania University, Hyderabad, India

[2] Department of Physics, BVRIT Hyderabad College of Engineering for Women, Hyderabad, India

Beta vulgaris (beetroot) and *Syzygium cumini* (black plum). *Syzygium cumini* dye extract has been shown to contain anthocyanin while beetroot contains betalains that are excellent light-harvesting pigments for the generation of charge carriers in the production of electricity.

2 Experimental procedure

2.1 Synthesis of ZnO and TiO_2 powders

The ZnO and TiO_2 nano crystallites were prepared by a microwave hydrothermal approach. For ZnO synthesis, firstly, 30 mL NaOH (3.2 mol/L) solution was slowly added to 30 mL $Zn(CH_3COO)_2{\cdot}2H_2O$ (1.6 mol/L) solution. For TiO_2 synthesis, 30 mL NaOH (3.2 mol/L) solution was slowly added into 30 mL $TiCl_4$ (1.6 mol/L) solution. These mixed solutions were transferred individually to a Teflon-lined autoclave of 50 mL capacity and then irradiated using a temperature controlled microwave synthesis system (MARS-5, CEM Corp., Mathews, NC, frequency 2.45 GHz, maximum power 1200 ± 50 W) at 180 °C for 45 min. After microwave reaction, the solution of the mixtures was cooled to room temperature. The resulting white precipitates were collected by filtration and washed with deionized water multiple times and then dried at 80 °C for 12 h in air.

2.2 Preparation of ZnO–TiO_2 composites

TiO_2–ZnO composites were prepared by mechanical mixing of synthesized ZnO and TiO_2 powders in the weight percentages defined as $(100-x)$ $TiO_2 + x(ZnO)$, where the weight percentages are $x = 0$, 10, 30, 50, 70, 90 and 100%. In general, TiO_2 exists in three phases: anatase, rutile and brookite. Pure brookite phase is unstable and difficult to synthesize. Pure rutile phase has limited photoactivity, and, therefore, is less photo efficient than anatase phase. For the application of TiO_2 in photocatalysis and DSSC, anatase phase of TiO_2 is considered to be more active. To attain the anatase phase of TiO_2 in composite samples, mixed powders were microwave heated at 550 °C for 90 min in the air atmosphere using a multimode cavity of 2.45 GHz microwave oven.

2.3 Natural dye extraction

A fresh *Syzygium cumini*/*Beta vulgaris* were cut into small pieces and soaked in 150 mL acetone (1:15 ratio) with stirring for 12 h at room temperature. The crude solution was filtered using filter paper to remove solid residue. Finally, the filtrate was washed multiple times with hexane to remove any oil or chlorophyll present in the extract and shielded from exposure to direct light and stored in a refrigerator at 5 °C.

2.4 Preparation of dye-sensitized solar cells

Fluorine doped tin oxide (FTO; Techinstro) conductive glass sheets were first cleaned by dipping it in detergent solution for 10 min, then sonicated using an ultrasonic bath for 5 min, rinsed with deionized water and then dried. Photoelectrodes were prepared on FTO glass slide via doctor blade technique with a glass slide and scotch tape as a spacer. To make a homogeneous slurry, prepared nanocomposite powders were mixed with water, acetylacetone and Triton-X 100 in pestle and mortar. Using this slurry, thin films of area 1.0 cm × 1.0 cm were prepared, dried at room temperature, followed by annealing at 450 °C for 30 min. For sensitization, the fabricated electrodes were dipped in natural dye (*Syzygium cumini*/*Beta vulgaris*) solution for 24 h. The counter electrode was made by spin coating 5 mmol/L $H_2PtCl_6{\cdot}6H_2O$ (Chloroplatinic acid hexahydrate) in isopropyl alcohol on FTO glass and sintering it at 385 °C for 15 min. For the complete fabrication of DSSC, the sensitized electrode and the counter electrode was assembled and a few drops of electrolyte, comprising of Li, I_2, TBP and TBAI in acetonitrile, were injected in between the electrodes.

2.5 Characterization

The phase identification of as-synthesized (TiO_2, ZnO) and composite (ZnO–TiO_2) powders was carried out using X-ray diffractometer [(XRD), Philips PW 1830] using CuKα radiation with $\lambda = 0.15418$ nm. The morphological characterization of synthesized and composite samples was determined using TEM (Jeol, JEM 2100) and FESEM [(FESEM), Carl Zeiss EVO 18] respectively. The quantitative elemental composition analysis has been carried out using energy dispersive X-ray spectroscopy (EDAX; OXFORD analytical). The optical properties of composite powders were examined via UV–Visible spectrophotometer (Shimadzu Uv 1800) and photoluminescence spectra (Fluorolog 3, Horiba Jobin-Yvon). Photoluminescence (PL) spectra of the TiO_2–ZnO composites have been recorded using a 450 W xenon lamp equipped with a Fluorolog 3, Horiba Jobin-Yvon fluorescence spectrometer at an excitation wavelength of 325 nm. Photocurrent density–voltage (J–V) characteristics of the developed DSSC have been measured under simulated solar light (AM 1.5 solar simulator, Newport, Model 96000) with Xe lamp and source meter (Keithley, Model 2400).

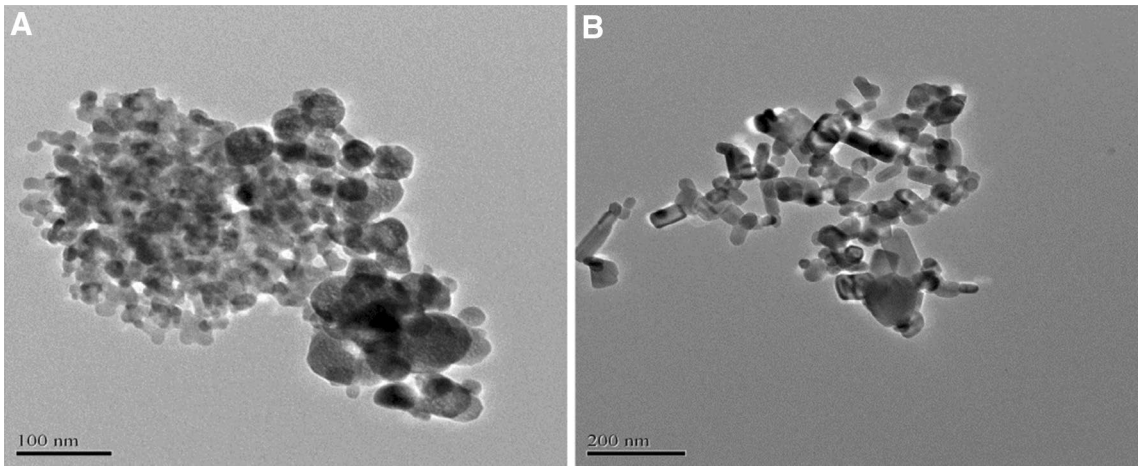

Fig. 1 TEM images of synthesized **a** TiO_2, **b** ZnO powders

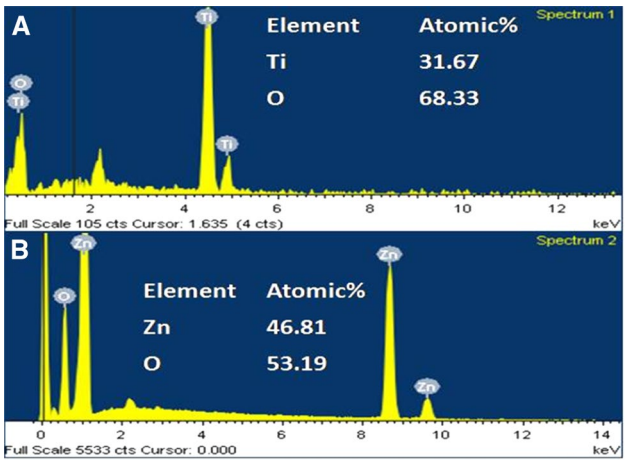

Fig. 2 Energy dispersive analysis (EDAX) of **a** TiO_2, **b** ZnO powders

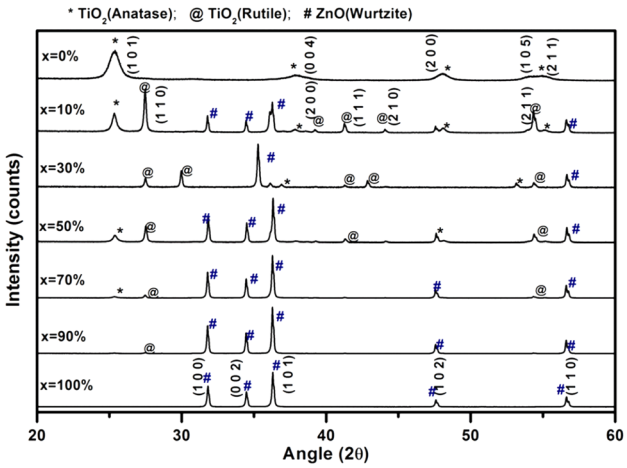

Fig. 3 Powder X-ray (Cu Kα radiation) diffraction patterns of $(100-x)\ TiO_2 + x(ZnO)$ composite samples

3 Results and discussions

Figure 1a, b show the TEM images of microwave hydrothermal synthesized TiO_2 and ZnO nanoparticles. It can be seen from the figure that the powder particles are uniform and of nearly spherical in shape in TiO_2 whereas ZnO nanoparticles have mixed morphology of spherical and elongated rod shape. It was revealed that the particle sizes of the TiO_2 and ZnO were 12 and 19 nm respectively. The elemental compositions of the synthesized powders were investigated via FESEM–EDX. The results of EDX analysis are shown in Fig. 2 and confirmed the presence of titanium and zinc, corresponding to the primary elements present in TiO_2 and ZnO powders, respectively.

Figure 3 shows the X-ray diffraction patterns of $(100-x)\ TiO_2 + x(ZnO)$ composite samples. From the Figure, it can be observed that the prepared TiO_2 and ZnO powders shown pure anatase phase (JCPDS No.: 84-1286) and the wurtzite phase (JCPDS No. 36-1451) respectively. Compared to the monocomponent nanomaterials (TiO_2 or ZnO), the nanocomposites indeed consist of wurtzite ZnO along with both anatase TiO_2 and rutile TiO_2 which is clearly shown in the XRD pattern. The sharp peaks observed from XRD patterns confirm the formation of highly crystalline phases. Furthermore, with the increase of the ZnO concentration, the characteristic peaks of anatase TiO_2 gradually decreased, and the characteristic peaks of wurtzite ZnO gradually increased in contrast. These XRD results further confirmed the successful preparation of the nanocomposites consisting of both TiO_2 and ZnO phases.

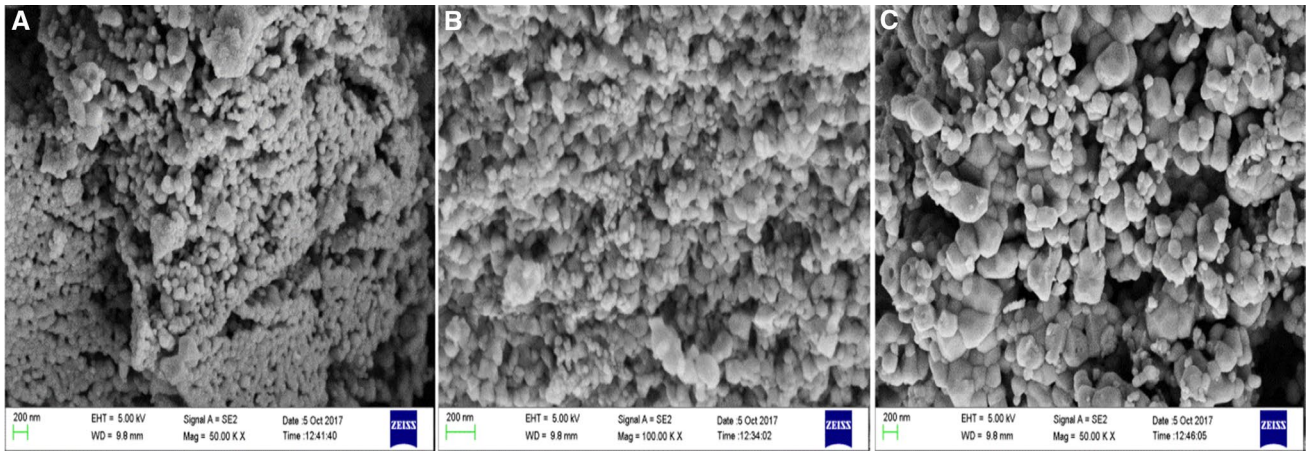

Fig. 4 FE-SEM images of $(100-x)TiO_2 + (x)ZnO$ composite electrodes **a** x = 0%, **b** x = 50% and **c** x = 100%

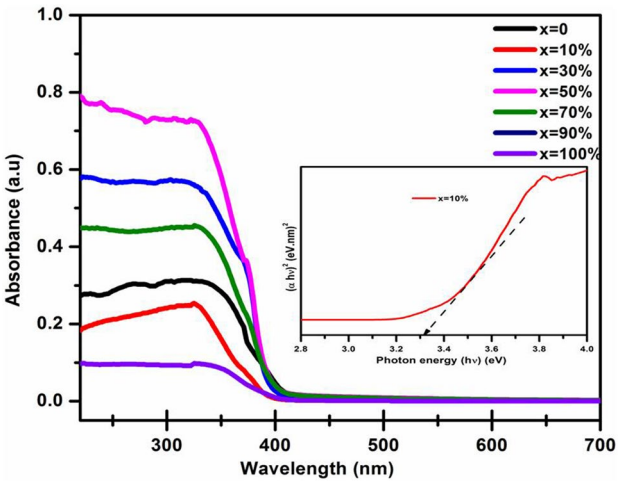

Fig. 5 UV–Vis absorption spectra of $(100-x)TiO_2 + (x)ZnO$ composites

Table 1 Bandgap energy values of $(100-x)TiO_2 + (x)ZnO$ composite samples

Sample (%)	Bandgap energy (Eg)
x = 0	3.26
x = 10	3.28
x = 30	3.30
x = 50	3.31
x = 70	3.36
x = 90	3.39
x = 100	3.24

The efficiency of catalysis is dependent on the surface morphology of nanoparticles. The fine spherical particle in anatase phase of TiO_2 in comparison with large, ragged and needle shape particle in rutile phase provided higher surface area [20]. Figure 4 shows FESEM images of the three typical composite electrodes (x = 0, x = 50% and x = 100%). From the images, it can be observed that the pure and composite electrodes exhibit the uniform spherical topography with high porous structure. This highly porous structure helps to attach more dye molecules on the surface of composite electrodes,and as on when the dye on the surface of particles of TiO_2–ZnO absorbs the light (photons) it results in excitation of more electrons. The particle size of the pure and composite powders was determined using line intercept method and it is found to be in the range 45–80 nm.

Figure 5 shows the UV–Vis absorption spectra of TiO_2–ZnO nanocomposite samples. In a semiconductor such as TiO_2 and ZnO, light is only absorbed if it has energy that is greater than the energy required to excite an electron from the valence band to the conduction band of the material. ZnO is a direct band gap semiconductor with bandgap energy around 3.3 eV. On the other hand, the TiO_2 is an indirect bandgap semiconductor with bandgap energy around 3.2 eV (387.5 nm) for anatase. From the figure,it can be observed that the present investigated samples are exhibiting transparent behaviour in the visible range (400–1000 nm). Moreover, for light wavelengths below 400 nm, the absorbance nature of samples are high and the percentage of absorption is varies with composition and it is maximum for x = 30 and 50% samples. In fact, the Zn atoms create distortion in TiO_2 lattice and in Ti–O bond length which causes shift in the absorption edge [21]. The average optical transmission of all the samples in the visible range part of the spectrum is found to be around 93%. Surface morphology has a significant effect on the optical properties of the sample. Larger pores of investigated samples result in the reduction of light scattering, which can decrease the absorbance of samples. From figure, itcan also be observed that UV spectra of composite samples showing the two absorption edges which can be attributed to the optical absorption of two crystalline phases. The optical band gap (E_g)

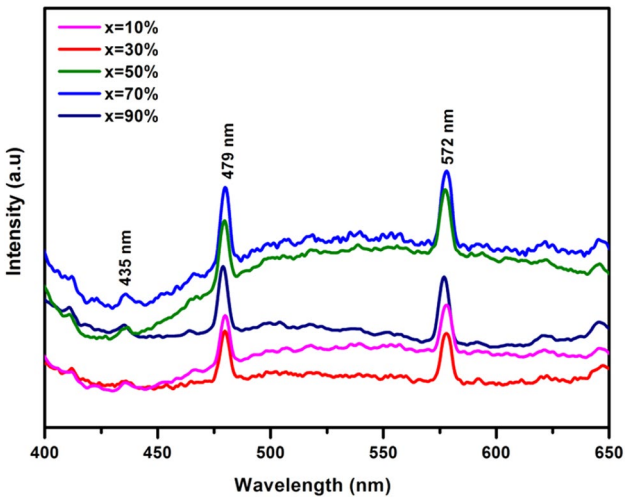

Fig. 6 PL spectra of $(100-x)TiO_2 + (x)ZnO$ composites

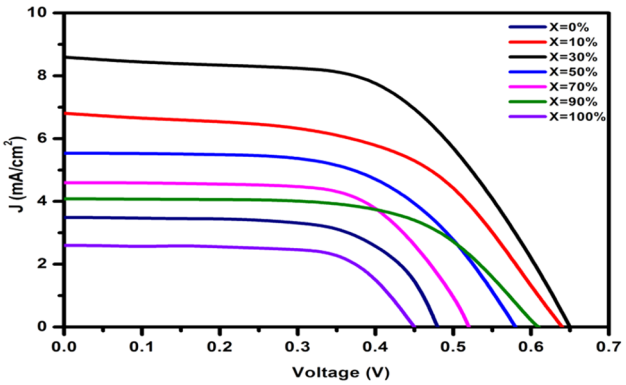

Fig. 7 J–V characteristics of the DSSCs made from $(100-x)$ TiO_2 + (x)ZnO composite photoanode and *Syzygium cumini* dye as photosensitizer

of investigated samples are measured from the plots $(\alpha h\upsilon)^2$ versus the photon energy ($h\upsilon$) and the obtained values of E_g are reported in Table 1. From the table, it can be seen that the composite samples band gap slightly higher compare to pure TiO_2 and ZnO samples.

Figure 6 shows typical PL spectra forcomposite samples with a xenon lamp excitation as a source. It can be seen from the figure that all the composite powders having similar exciton PL peaks (435, 479 and 572 nm) behaviour however, the PL intensity varies with composition. The similar emission behavior of the PL spectra indicates that all the composite samples have a similar origin of PL emission. Ingeneral, PL spectra of TiO_2 materials are attributed to three types of physical origins: self trapped excitons, oxygen vacancies, and surface states [22]. The peak at around 435 nm in the blue-violet region originates from charge recombination in the surface state defects. These surface states are possible due to the interaction of ZnO and TiO_2. The bands at around 479 nm in the blue area are due to different intrinsic defects in the TiO_2 lattice such as oxygen vacancies, titanium vacancies and interstitial defects. A green emission can be seen at around 572 nm which may be due to electron–hole recombination. The variation in PL intensity indicates that the rate of recombination of electron- hole varies from sample to sample. From the figure, it can be observed that the PL spectra intensity of x = 10 and x = 30% is low when it is compared to other samples, which indicates that the samples with x = 10 and x = 30% ZnO composite samples have low rate of recombination compare to other samples.

Figures 7 and 8 show the measured current density (J) and voltage (V) characteristics of the TiO_2–ZnO composite photoanode DSSCs with *Syzygium cumini* and *Beta vulgaris* dyes respectively. Photovoltaic tests of DSSC with these natural dyes as sensitizers were performed by measuring the current density and voltage (J–V) characteristics under irradiation with white light (100 mW cm^{-2} from 300 W solar simulator). The performance of natural dyes as sensitizers in DSSCs was evaluated by short-circuit current (J_{sc}), open circuit voltage (V_{oc}), fill factor (FF) and energy conversion efficiency (η) parameters and obtained results are listed in Tables 2 and 3. A η of 1.05% was achieved for the *Syzygium cumini* dye pristine TiO_2 photoanode DSSC, with a J_{sc} of 3.45 mA/cm^2, a V_{oc} of 0.47 V and a FF of 63.83. Besides a η of 2.73% was achieved for the *Beta vulgaris* dye pristine TiO_2 photoanode DSSC, with a J_{sc} of 6 mA/cm^2, a V_{oc} of 0.86 V and a FF of 52.9. From the table, it can be observed that with increasing of ZnO(x) concentration in $(100-x)$ TiO_2 + (x)ZnO composites all the parameters (J_{sc}, V_{oc}, FF and η) vary and no systematic behaviour is observed. The increase in photocurrent with low amount ZnO concentration can be attributed to rapid electron transport and the

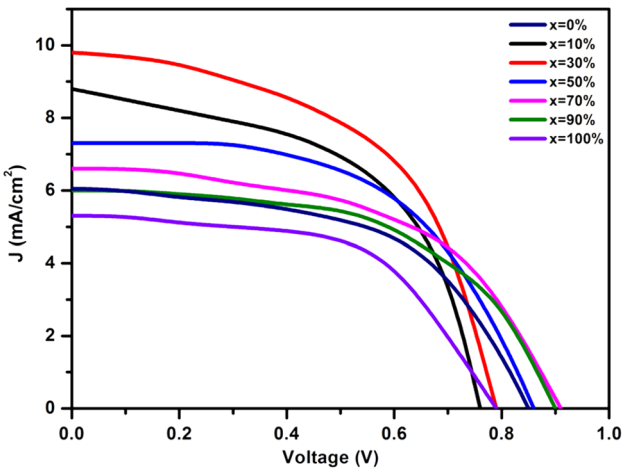

Fig. 8 J–V characteristics of the DSSCs made from $(100-x)$ TiO_2 + (x)ZnO composite photoanode and *Beta vulgaris* dye as photosensitizer

Table 2 Photovoltaic performances of the DSSCs made from $(100-x)TiO_2 + (x)$ ZnO composite photoanode and *Syzygium cumini* dye as photosensitizer

Sample (%)	J_{sc} (mA/cm^2)	J_{max} (mA/cm^2)	V_{max} (V)	V_{oc} (V)	FF (%)	η (%)
x = 0	3.45	3.0	0.35	0.47	63.83	1.05
x = 10	6.82	7.8	0.44	0.64	71.69	3.12
x = 30	8.3	8.0	0.42	0.65	62.22	3.35
x = 50	5.52	5.0	0.38	0.58	59.56	1.89
x = 70	4.57	4.25	0.36	0.52	65.38	1.53
x = 90	4.10	3.8	0.40	0.61	60.77	1.52
x = 100	2.65	2.1	0.35	0.45	72.59	0.85

Table 3 Photovoltaic performances of the DSSCs made from $(100-x)TiO_2 + (x)$ ZnO composite photoanode and *Beta vulgaris* dye as photosensitizer

Sample (%)	J_{sc} (mA/cm^2)	J_{max} (mA/cm^2)	V_{max} (V)	V_{oc} (V)	FF (%)	η (%)
x = 0	6.0	4.2	0.65	0.86	52.90	2.73
x = 10	8.7	6.5	0.61	0.76	59.96	3.96
x = 30	9.8	7.1	0.63	0.79	57.77	4.47
x = 50	7.3	6.1	0.60	0.88	56.97	3.66
x = 70	6.5	4.8	0.68	0.90	55.79	3.26
x = 90	6.0	5	0.65	0.91	59.62	3.25
x = 100	5.4	4.2	0.59	0.80	57.36	2.48

shortened electron-transfer distance. Moreover, the Voc improved with the ZnO concentration up to 30% owing to the suppression of electron recombination, consequently improving the conversion efficiency. However, when a higher ZnO concentration was introduced, J_{sc} decreased because higher ZnO concentrations formation of the Zn^{2+}/dye complexes, which hinder dye absorption, electron transport and electrolyte penetration. Consequently, the DSSCs that used x = 10 and x = 30% of $(100-x)TiO_2 + (x)ZnO$ photoanodes exhibited more than double efficiency compare to that of pure TiO_2 and ZnO based DSSC efficiency irrespective of dye. In both *Syzygium cumini* and *Beta vulgaris* dye based series, x = 30% photoanode DSSC showing the highest efficiency 3.35 and 4.47% respectively. The obtained efficieny values of present investigate TiO_2–ZnO DSSC is superior compare to several composite photoanode reports. Tripathi and Chawla [23] noted that the efficiency of betacyanin sensitized CeO_2–TiO_2 composite photoanode DDSC increases from 0.63 to 2.8% with CeO_2 concentration. Jiao et al. [24] deposited layers of nano-sized MgO on TiO_2 nanowires.According to their results, the short circuit current of the cell improved 35% and the efficiency of the cell rose from 1.11 to 1.37%.

4 Conclusions

Dye sensitized solar cells are successfully fabricated with TiO_2–ZnO composite photoanode and natural (*Syzygium cumini* and *Beta vulgaris*) sensitizers. Then the cell performance of sensitized solar cell is investigated using J_{sc}, V_{oc}, FFand η parametsrs. From these studies, it may be concluded that the addition of ZnO to TiO_2 enhances the cell performance due to the reduced recombination of photoinjected electrons. The *Beta vulgaris* dye has higher photosensitized performance compare to *Syzygium cumini* due to the better charge transfer between the betacyanin dye molecule and the TiO_2–ZnO surface that is related to a dye structure. Hence, this dye provides a more efficient incidentphoton to electron conversion.

References

1. K. Fan, J. Yu, W. Ho, Mater. Horiz. **4**, 319–344 (2017)
2. Z. Huizhi, L. Wu, Y. Gao, T. Ma, Dye-sensitized solar cells using 20 natural dyes as sensitizers. J. PhotochemPhotobiol. A Chem. **219**, 188–194 (2011)
3. S. Shalini, R. BalasundaraPrabhu, S. Prasanna, T.K. Mallick, S. Senthilarasu, Review on natural dye sensitized solar cells: operation, materials and methods. Renew. Sustain. Energy Rev. **51**, 1306–1325 (2015)
4. B. O'Regan, M. Gratzel, A low-cost, high-efficiency solar cell based on dye-sensitized colloidal TiO_2 films. Nature **353**, 737–740 (1991)
5. J. Lim, M. Lee, S.K. Balasingam, J. Kim, D. Kim, Y. Jun, Fabrication of panchromatic dye-sensitized solar cells using pre-dye coated TiO_2 nanoparticles by a simple dip coating technique. RSC Adv. **3**, 4801–4805 (2013)
6. K.E. Jasim, *Dye Sensitized Solar Cells—Working Principles, Challenges and Opportunities, in Solar Cells—Dye-Sensitized Devices*, ed. L. A. Kosyachenko (InTech, 2011)
7. J. Gong, K. Sumathy, Q. Qiao, Z. Zhou, Review on dye-sensitized solar cells (DSSCs): advanced techniques and research trends. Renew. Sustain. Energy Rev. **68**, 234–246 (2017)

8. X.L. Mao, R. Zhou, S.W. Zhang, L.P. Ding, L. Wan, S.X. Qin, Z.S. Chen, J.Z. Xu, S.D. Miao, High efficiency dye-sensitized solar cells constructed with composites of TiO_2 and the hot-bubbling synthesized ultra-small SnO_2 nanocrystals. Sci. Rep. **6**, 19390 (2016)
9. A. Zaban, S.G. Chen, S. Chappel, B.A. Gregg, Bilayer nanoporous electrodes for dye sensitized solar cells. Chem. Commun. **22**, 2231–2232 (2000)
10. D. Maheswari, P. Venkatachalam, Enhanced performance of bi-layer Nb_2O_5 coated TiO_2 nanoparticles/nanowires composite photoanode in dye-sensitized solar cells. Photonica Nanostruct. Fundam. Appl. **12**(5), 515–526 (2014)
11. R. Kushwaha, P. Srivastava, L. Bahadur, Natural pigments from plants used as sensitizers for TiO_2 based dye-sensitized solar cells J. Energy (2013). https://doi.org/10.1155/2013/654953
12. M.R. Narayan, Review: Dye sensitized solar cells based on natural photosensitizers. Renew. Sustain. Energy Rev. **16**, 208–215 (2012)
13. M. Maaza, *Natural Dyes for Photonics Applications*, (Wiley, Chichester, 2014)
14. A. Mbonyiryivuze, I. Omollo, B.D. Ngom, B. Mwakikunga, S.M. Dhlamini, Natural dye sensitizer for gratzel cells: sepia melanin. Phys. Mater. Chem. **6**, 1–6 (2015)
15. J.F. Lei, S.L. Liu, K. Du, S.J. Lv, C.J. Liu, L.Z. Zhao, ZnO@ TiO_2 architectures for a high efficiency dye-sensitized solar cell. Electrochim. Acta **17**, 66–71 (2015)
16. Q. Wali, Z.H. Bakr, N.A. Manshor, A. Fakharuddin, R. Jose, SnO_2–TiO_2 hybrid nanofibers for efficient dye-sensitized solar cells, solar energy. Sol. Energy **132**, 395–404 (2016)
17. R. Milan, G.S. Selopal, M. Epifani, M.M. Natile, G. Sberveglieri, A. Vomiero, I. Concina, ZnO@SnO_2 engineered composite photoanodes for dye sensitized solar cells. Sci. Rep. **5**, 14523 (2015)
18. Y.S. Wang, T.T. Chen, Y.J. Huang, T.P. Huang, Y.Y. Lee, H.T. Chiu, C.Y. Lee, $SrTiO_3$/TiO_2 hybridstructure as photoanode in dye-sensitized solar cell. J. Chin. Chem. Soc. **60**(12), 1437–1441 (2013)
19. M. Yang, B. Dong, X. Yang, W. Xiang, Z. Ye, E. Wang, L. Wan, L. Zhao, S. Wang, TiO_2 nanoparticle/nanofiber-ZnOphotoanode for the enhancement of the efficiency of dyesensitized solar cells. RSC Adv. **7**, 41738 (2017)
20. M. Andersson, L.O. sterlund, S. Ljungstrom, A. Palmqvist, Preparation of nanosizeanatase and rutile TiO_2 by hydrothermal treatment of microemulsions and their activity for photocatalytic wet oxidation of phenol. J. Phys. Chem. B **106**, 10674–10679 (2002)
21. S. Ayed, R.B. Belgacem, J.O. Zayani, A. Matoussi, Structural and optical properties of ZnO/TiO_2 composites. Superlattice Microstruct. **91**, 118–128 (2016)
22. K. Anbalagan, UV-sensitized generation of phasepure cobalt-doped anatase: $Co_xTi_{1-x}O_{2-\delta}$ nanocrystals with ferromagnetic behavior using Nano-TiO_2/cis-$[Co^{III}(en)_2(MeNH_2)Cl]^{2+}$. J. Phys. Chem. C **115**, 3821–3832 (2011)
23. M. Tripathi, P. Chawla, CeO_2-TiO_2photoanode for solid state natural dye-sensitized solar cell. Ionics **21**, 541–546, (2015)
24. X.J. Jiao, H. Lin, D.T. Zhuang, X. Li, J.B. Li, Fabrication of MgO-coated TiO_2 nanowires films and applicationin dye-sensitized solar cells. Rare Metal Mat. Eng. **40**, 318–321 (2011)